ELSEVIER

Catalysis Today 38 (1997) 39–46

CATALYSIS TODAY

3-D modeling of monolith reactors

Robert Jahn, Dalimil Šnita, Milan Kubíček, Miloš Marek*

Prague Institute of Chemical Technology, Technická 5, 166 28 Prague 6, Czech Republic

Abstract

Dynamic behavior of a monolith catalytic reactor formed by ceramic body with the system of parallel channels with square crossection has been studied experimentally and by numerical simulation. Gaseous reaction mixture flows through channels without mass exchange among them. Inner channel surface is coated with catalyst and strongly exothermic reaction of CO oxidation takes place on the catalyst surface. Constructed experimental monolith reactor enables measurement of temperature profiles along 24 chosen channels. The used three-dimensional (3D) model considers heat conduction and accumulation in the solid phase (Fourier equation) and mass and heat balances both on the surface of the catalyst and in the gas phase. Proper discretization of concentration and temperature fields leads to a system of several tens of thousands of ODE's which are then integrated on a fast workstation. Mutual interaction of heat accumulation, heat transfer and nonlinear heat generation gives rise to propagating temperature fronts. Evolution of temperature fields for spontaneous ignition and extinction and after electric preheating of small part of the monolith are studied experimentally and by mathematical modeling.

Keywords: Modeling, 3-D; Monolith reactor; Dynamic

1. Introduction

Transient behavior of catalytic monolith reactors still remains the subject of interest, even if they have been used on a large scale in automobile emission control since 1975. Monolithic catalytic reactors are now being used not only for VOC abatement in a gas phase, but also they have been studied for the use in three phase catalytic reactors [1]. If the flow distribution at the monolith inlet is nonuniform, or there is nonuniform distribution of catalytic activity among monolith channels, then there exist severe radial temperature gradients even under adiabatic conditions. The problem of description of two and three dimensional (2D and 3D) spatiotemporal patterns in the monolith has been discussed in several papers. Aris [2] pointed out that models combining two-dimensional single-channel models to study the transient behavior of monolith reactors containing several thousands of thermally interacting channels are numerically intractable. He introduced an equivalent continuum approach which has been later used to study thermal interaction among adjoining monolith channels [3,4]. Single partial differential equation modeling the heat transfer in solid walls of the entire monolith is derived from the simplified difference–differential equations describing thermal interactions among adjoining channels. The coefficients of this equation provide the effective axial and radial thermal conductivities for solid phase of the homogenized medium. Flytzani-Stephanopulos et al. [5] have studied heat transfer in metal honeycomb monolith with-

*Corresponding author. e-mail: marek@vscht.cz

PII S0920-5861(97)00037-0

out reaction and compared it with the situation in the packed bed of ceramic pellets. A transient three-dimensional model including the effects of the transverse heat flux and nonuniform gas flow distribution based on the equivalent continuum approach was described by Chen et al. [6] and used to study behavior of simulated automobile convertor.

We have recently constructed an experimental system consisting of ceramic monolithic catalytic reactor with the possibility of observation of longitudinal temperature profiles along 24 individual channels and used it for the measurement of ignition phenomena and observation of transient thermal wave propagation in the catalytic CO oxidation over Pt–Rh commercial catalyst. The results are described in the first part of the paper. The possibility of measurement of temperature profiles in individual monolith channels substantiates the development of a class of detailed multichannel monolith models which are not based on the equivalent continuum approach. Two types of such models are described in the second part of the paper.

2. Experimental

To enable detailed studies of the development of spatiotemporal temperature profiles in the monolithic reactor during the course of the ignition under chosen conditions in the entire monolith (local heating, inlet distribution), the experimental equipment schematically shown in Fig. 1 was constructed [7]. The equipment consists of two parts. The lower part (the reactor module) is well insulated (HI), sustains high temperatures and contains the monolithic reactor with the thermocouples inserted into individual channels. The upper part of the reactor, the thermocouple positioning mechanism with the stepping motor (SM) and the inner and the outer capillaries IC and OC used for the positioning of the thermocouples (TC) is PC controlled and enables programmed measurement of longitudinal temperature profiles in chosen channels. Thin fast response thermocouples has to stop for about 2 s at each measuring position so as to avoid the effects of the thermocouples transient on the measured value of temperatures. The position of thermocouples in individual channels with the corresponding dimensions is schematically shown in Fig. 2.

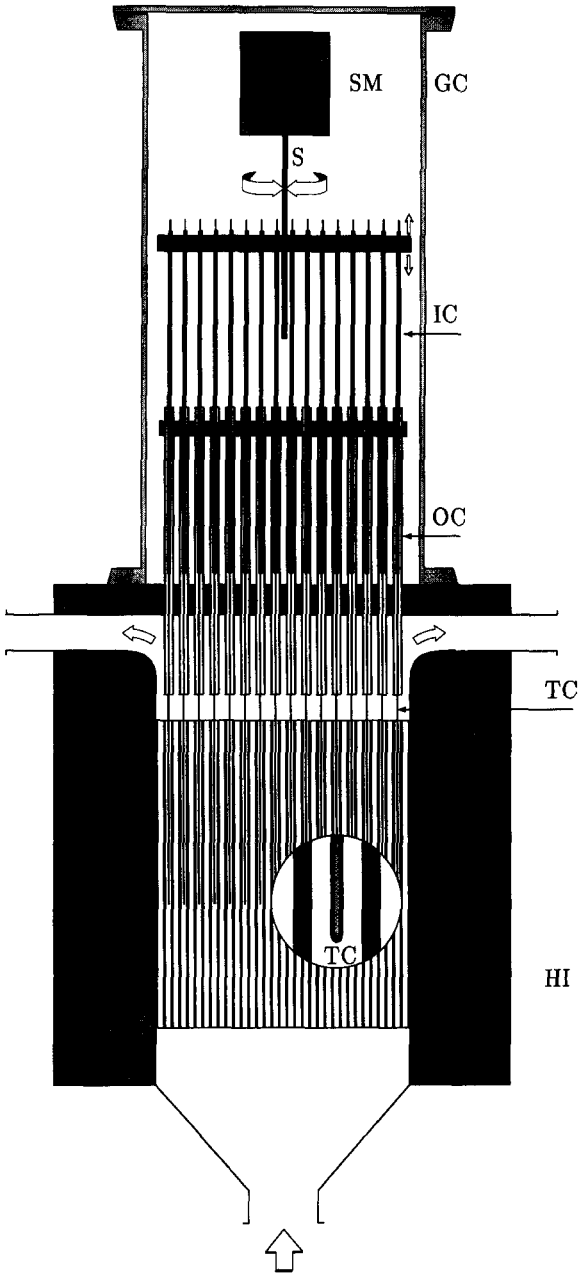

Fig. 1. Experimental reactor with thermocouples (TC) for measurement of temperature field: SM, stepping motor; S, screw; IC, inner capillary; OC, outer capillary; GC, glass cylinder; HI, heat insulation.

CO oxidation reaction (equimolar mixture with O_2, rest N_2) on the Pt/Rh (5 : 1) commercial monolith catalysts (diameter 5 cm, length 12 cm) was studied.

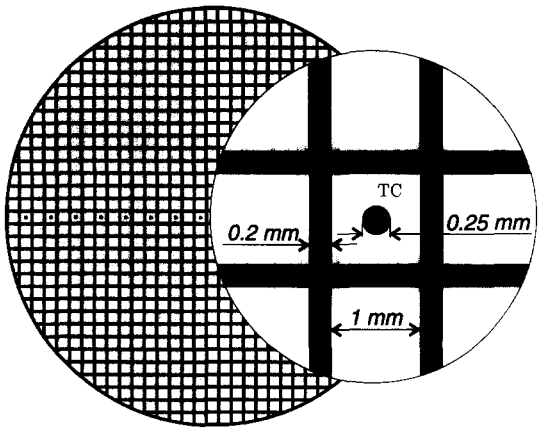

Fig. 2. Crossection of experimental reactor with thermocouples (TC) for measurement of temperature field.

The outlet concentrations of CO and CO_2 were measured by infrared analyzers [8]. Thermocouples of 0.25 mm diameter occupy 9.6% of the channel crossection area (Fig. 2). Temperature values obtained from 24 thermocouples which can be shifted along the channels are stored on the PC.

The spatiotemporal temperature patterns presented correspond to specific experimental situation with relatively low gas flow 2 l min^{-1}, hence the temperature transients are slow. Order of magnitude higher flow rates are being studied now. Typical times in temperature transients in monolithic catalysts used in automobile exhaust afterburners are of the order of minutes.

The evolution of measured temperature profiles in the monolith along the x-axis (length) and y-axis (radial direction) in the course of spontaneous ignition and reaction front propagation when the inlet gas temperature is slightly above the catalyst light-off temperature is depicted in Fig. 3. The ignition starts at the center of the reactor; the formed hot reaction front then begins to propagate to the face of the monolith and finally stationary state with the temperature maximum approximately 1.5 cm from the face is established. The inserted figures show the time course of the average outlet conversion ξ where the dot denotes actual position in time (similarly as in the following Fig. 4).

The evolution of temperature profiles in the course of spontaneous extinction of the reaction following

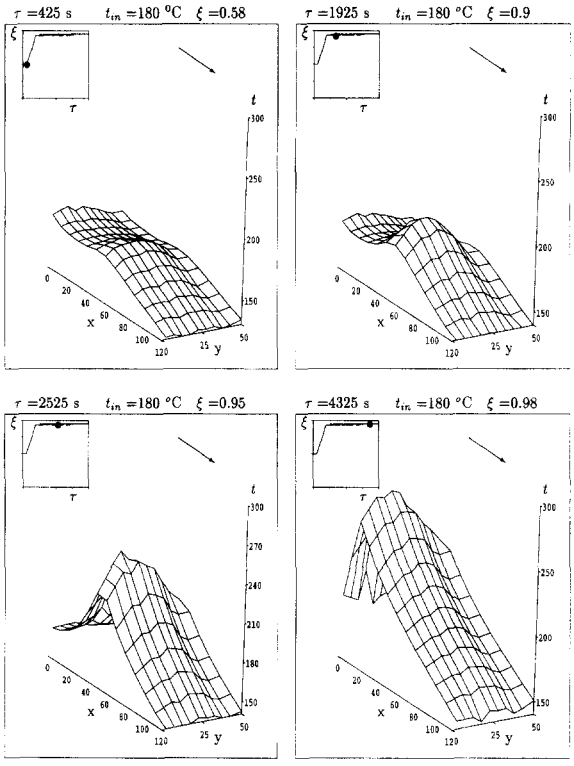

Fig. 3. Measured evolution of spatial temperature t(°C) profiles during spontaneous ignition with the inlet gas temperature only slightly above the catalyst light-off temperature. t_{in}=180°C; inlet CO concentration=4% vol.; → denotes flow direction; x, axial coordinate (mm); y, radial coordinate (mm); ξ, averaged outlet conversion; τ, time.

the gradual decrease of the inlet temperature is shown in Fig. 4. The hot zone which was originally located approximately 3 cm from the face of the monolith is subsequently shifted to the outlet, the maximum at the same time decreases until the final state with flat temperature field and low conversion is reached.

The successful attempt to ignite the reaction by electric heating of the central part of the monolith, realized by resistance wires located in the central four channels (Fig. 5) is shown in Fig. 6. The heating was applied for 440 s and the temperature reached was ca 700°C. When the heating was switched off, the ignited hot reaction front propagated from the center to the perimeter of the reactor and became stationary close to the monolith inlet. The stationary state with high conversion was reached.

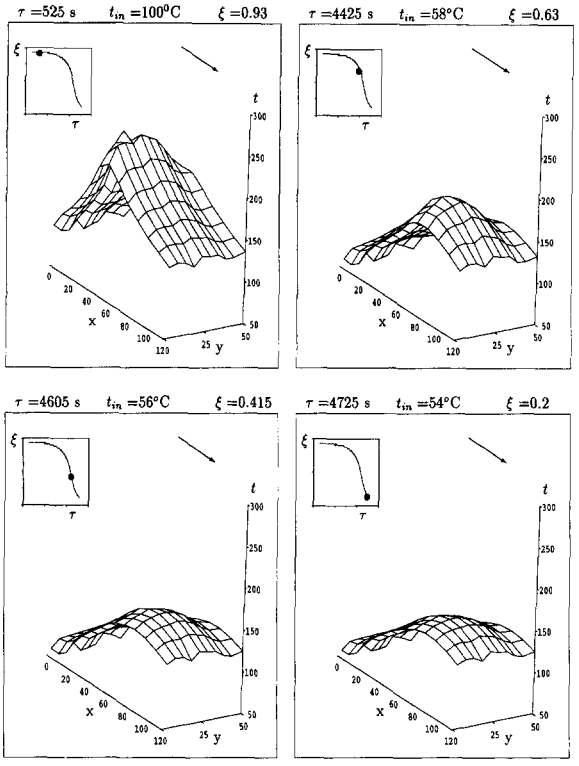

Fig. 4. Measured evolution of spatial temperature (°C) profiles during spontaneous extinction with slowly decreasing (approx. 1°C per 100 s) inlet gas temperature into the monolith. Inlet CO concentration=4% vol.; → denotes flow direction; x, axial coordinate (mm); y, radial coordinate (mm); ξ, averaged outlet conversion; τ, time.

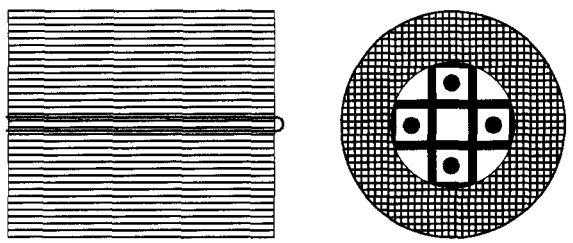

Fig. 5. Arrangement of resistance electric heating elements in the center of the monolith.

3. Two-phase 3D model

Let us assume that the solid phase is impermeable for gaseous components, the direction of flow of reaction mixture is parallel to the x-axis and the catalytic surface is perpendicular to the y–z plane. The heat balance

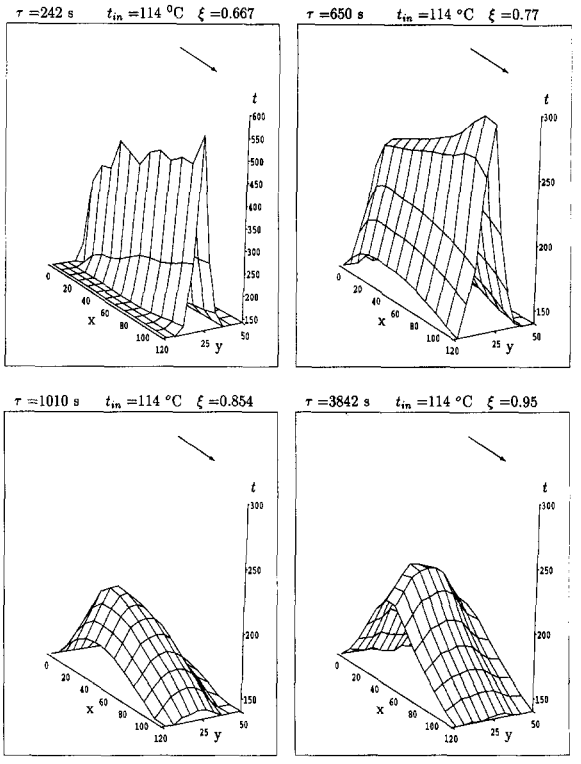

Fig. 6. Temperature profiles (°C) developing after resistance electric heating applied at the centre of the monolith (Fig. 5) at the inlet to the monolith. Inlet CO concentration=4% vol. → denotes flow direction; x, axial coordinate (mm); y, radial coordinate (mm); ξ, averaged outlet conversion; τ, time.

$$\frac{\partial t_s}{\partial \tau} = \frac{\lambda_s}{\rho_s c_{ps}} \left(\frac{\partial^2 t_s}{\partial x^2} + \frac{\partial^2 t_s}{\partial y^2} + \frac{\partial^2 t_s}{\partial z^2} \right), \quad (x,y,z) \in V_s \qquad (1)$$

describes temperature field in the space region occupied by the solid phase. Here t_s is the solid phase temperature, λ_s is thermal conductivity of the solid phase, ρ_s is the density of the solid phase and c_{ps} is heat capacity of the solid phase. The mass and heat balances in the gas phase are

$$\frac{\partial t_g}{\partial \tau} = -v_x \frac{\partial t_g}{\partial x} + \frac{\lambda_g}{\rho_g c_{pg}} \left(\frac{\partial^2 t_g}{\partial x^2} + \frac{\partial^2 t_g}{\partial y^2} + \frac{\partial^2 t_g}{\partial z^2} \right), \quad (x,y,z) \in V_g \qquad (2)$$

$$\frac{\partial c_i}{\partial \tau} = -\frac{\partial}{\partial x}(v_x c_i) + D_i \left(\frac{\partial^2 c_i}{\partial x^2} + \frac{\partial^2 c_i}{\partial y^2} + \frac{\partial^2 c_i}{\partial z^2} \right), \quad (x,y,z) \in V_g \qquad (3)$$

Here c_i, i=1,...,N is molar concentration of the i-th component in the gas phase, N is the number of

components, v_x is the velocity of the gas phase in the direction of the x-axis, $D_i(t_g)$ is diffusion coefficient of the i-th component in the gas phase, t_g is the gas phase temperature, $\lambda_g(t_g)$ is thermal conductivity of the gas phase, $\rho_g(t_g)$ is the density of the gas phase, and c_{pg} is heat capacity of the gas phase. The mass and enthalpy balances on the catalytic surface (without accumulation) are defined on the interphase surface between the solid and the gas phase:

$$\lim_{g\to s} D_i \frac{\partial c_i}{\partial n_{gs}} = -\sum_{j=1}^{M} \nu_{i,j} r_j(c_{gs,1}, \ldots, c_{gs,N}, t_{gs}),$$
$$(x,y,z) \in A_{gs}, \tag{4}$$

$$\lim_{g\to s} \lambda_g \frac{\partial t_g}{\partial n_{gs}} = \sum_{j=1}^{M} \Delta H_{rj} r_j(c_{gs,1}, \ldots, c_{gs,N}, t_{gs})$$
$$+ \lim_{s\to g} \lambda_s \frac{\partial t_s}{\partial n_{gs}}, (x,y,z) \in A_{gs}, \tag{5}$$

Here $\partial/\partial n_{gs}$ is the normal derivative in the direction perpendicular to the catalytic surface oriented from the solid phase into the gas phase, $\lim_{s\to g}$ denotes values in the solid phase close to the solid-gas interface, $\lim_{g\to s}$ denotes values in the gas phase close to the gas-solid interface, $\nu_{i,j}$ is stoichiometric coefficient of the i-th component in the j-th chemical reaction, $r_j(c_{gs,1}, \ldots, c_{gs,N}, t_{gs})$ is the reaction rate of the j-th reaction (where $t_{gs} = \lim_{g\to s} t_g = \lim_{s\to g} t_s$ and $c_{gs,i} = \lim_{g\to s} c_i$), M is the number of chemical reactions and ΔH_{rj} is the heat of the j-th chemical reaction. The enthalpy balance on the solid-environment interface can be written in the form:

$$\alpha_b(t_s - t_b) = -\lim_{s\to b} \lambda_s \frac{\partial t_s}{\partial n_{sb}}, (x,y,z) \in A_{sb} \tag{6}$$

Here $\partial/\partial n_{sb}$ is normal derivative in the direction perpendicular to the external surface oriented from the solid phase into the environment, $\lim_{s\to b}$ denotes limit values in the solid phase close to the solid-environment interface, α_b is the heat transport coefficient and t_b is the temperature of the environment. The Navier-Stokes equation for stationary laminar non-isothermal flow in the channel can be written down in the following form:

$$\eta_g\left(\frac{\partial^2 v_x}{\partial y^2} + \frac{\partial^2 v_x}{\partial z^2}\right) + \frac{\partial \eta_g}{\partial y}\frac{\partial v_x}{\partial y} + \frac{\partial \eta_g}{\partial z}\frac{\partial v_x}{\partial z} = -\frac{\partial p}{\partial x},$$
$$(x,y,z) \in V_g \tag{7}$$

Here v_x is the velocity of the gas phase in the direction of the x-axis, $\eta_g(t_g)$ is the gas phase dynamic viscosity and p is pressure. The velocity at catalytic surface is equal to zero:

$$v_x = 0\ ,\ (x,y,z) \in A_{gs} \tag{8}$$

The above described model represents relatively general description of two phase reacting system. Numerical solution of the full model is extremely computer time expensive. Therefore, well founded simplifications can be introduced to obtain a more easily solvable model. One way of simplification, based on an averaging and pseudostationary description will be presented in the following paragraph, for other approaches see eg., [9].

4. Multichannel model: 3D in the solid phase, 1D pseudo-stationary plug flow in the gas phase in individual channels (MC3D1D)

Heat and mass fluxes from the gas phase to the catalytic surface in the k-th channel can be described by means of heat and mass transport coefficients:

$$-\lim_{g\to s} \lambda_g \frac{\partial t_g}{\partial n_{gs}} = \alpha_g^k(\hat{t}_g^k - t_{gs}),$$
$$-\lim_{g\to s} D_i \frac{\partial c_i}{\partial n_{gs}} = \beta_i^k(\hat{c}_i^k - c_{gs,i}), (x,y,z) \in A_{gs}^k; \tag{9}$$

here $\hat{t}_g^k$ and $\hat{c}_i^k$ are average values of temperature and concentration over the crossection of the k-th channel, respectively, and A_{gs}^k is the interphase surface between the gas phase and the solid phase in the k-th channel. Using additional assumption that the terms describing accumulation and axial mixing in the gas phase are negligible with respect to other terms in the balances [2,3] we then obtain for the gas phase in the k-th channel:

$$0 = -A_g^k \hat{\rho}_g^k \hat{v}_x^k \frac{d\hat{t}_g^k}{dx} + \int_{P_{gs}^k} \alpha_g^k(t_{gs} - \hat{t}_g^k) dp \tag{10}$$

$$0 = -A_g^k \frac{d}{dx}(\hat{v}_x^k \hat{c}_i^k) + \int_{P_{gs}^k} \beta_i^k(c_{gs,i} - \hat{c}_i^k) dp \tag{11}$$

here A_g^k is the area of crossection of the k-th channel, P_{gs}^k is the perimeter of the crossection of the k-th channel (Fig. 7), $\hat{v}_x^k$ and $\hat{\rho}_x^k$ are average values of

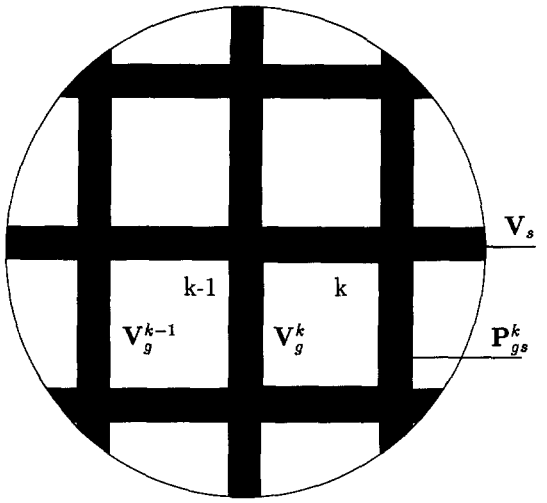

Fig. 7. Detail of the crossection of the monolith: V_s, solid phase; V_g^k, gas phase in the k-channel; P_{gs}^k, perimeter of the k-th channel; A, B and C, finite volumes of the solid phase formally related to the $(k-1)$-th channel; D, E and F, finite volumes of the solid phase formally related to the k-th channel; B and E, finite volumes without contact with the gas phase; A, C, D and F, finite volumes with contact with the gas phase.

velocity and density over the crossection of the k-th channel, respectively. For catalytic surface it holds:

$$\beta_i(\hat{c}_i^k - c_{gs,i}) = -\sum_{j=1}^{M} \nu_{i,j} r_j(c_{gs,1}, \ldots, c_{gs,N}, t_{gs}),$$
$$(x,y,z) \in A_{gs}^k, \tag{12}$$

$$\alpha(\hat{t}_g^k - t_{gs}) = \sum_{j=1}^{M} \Delta H_{rj} r_j(c_{gs,1}, \ldots, c_{gs,N}, t_{gs})$$
$$+ \lim_{s \to g} \lambda_s \frac{\partial t_s}{\partial n_{gs}}, (x,y,z) \in A_{gs}^k. \tag{13}$$

The studied model then consists of the following coupled set of differential-algebraic equations: PDE(1), $(N+1)$ ODE's Eqs. (10) and (11) and $(N+1)$ algebraic Eqs. (12) and (13).

Now we have to express the quantities α and β_i. The most simple approach is to consider α_g^k and β_i^k as empirical or semi-empirical quantities:

$$\alpha_g^k = \mathrm{Nu}^k \frac{\hat{\lambda}_g^k}{\delta}, \beta_i^k = \mathrm{Sh}^k \frac{\hat{D}_i^k}{\delta} \tag{14}$$

where Nu^k and Sh^k are the Nusselt and Sherwood number in the k-th channel, respectively, $\hat{\lambda}_g^k$ and $\hat{D}_i^k$ are average values of λ_g and D_i over crossection of the k-th channel, respectively, and δ denotes the characteristic channel dimension in the transverse direction. Another way of approach is to evaluate the heat and mass transport coefficients from numerical simulations of the full model for single channel with sufficiently accurate description of 3D fields in the gas phase.

From the state equation of the gas mixture we can further express

$$\hat{\rho}_g^k = \frac{p\hat{M}_g}{R\hat{T}_g^k}, \ \hat{v}_x^k = \frac{\dot{m}_g^k}{\hat{\rho}_g^k}, \tag{15}$$

where $\hat{M}_g$ is mean molecular mass of the gas, R is gas constant, $\hat{T}_g^k = \hat{t}_g^k + 273.15$ and $\dot{m}_k^g$ is mass flow through the k-th channel. This description is only an approximation with respect to the method of averaging over the channel crossection as the error of approximation increases with increasing temperature differences over the crossection.

5. Numerical methods

The partial differential Eq. (1) was transformed by means of spatial discretization into the system of ODEs (method of lines) and integrated by the one step explicit algorithm with the automatic step size control (Merson's modification of Runge-Kutta fourth order method). The spatial discretization was realized by the method of finite volumes (prisms) and implemented by means of the 'pre-processor-solver' approach. Each solid phase element has 6 neighboring elements which can belong either to solid phase, gas phase or the exterior part of the reactor. These possibilities are tested in the course of the pre-processor run, the elements are appropriately numbered and related to the others, and the part of the solver is generated. In the resulting code the testing is already avoided, all relations among the data structures are pre-defined and the constant terms are pre-computed. The solver code thus becomes efficient. Eq. (10) and Eq. (11) (ODEs in the spatial variable x for each channel) for the MC3D1D model are solved by the trapezoidal rule at each calling of the right-hand-sides of the set of ODEs integrated in time. The code for the trapezoidal rule is also pre-processed. Typical case of the simulation of one quarter of the monolith consist-

ing of K=200 parallel channels with J=100 steps in axial direction and N=1 using spatial discretization with L=3 elements of the solid phase per crossection of a single channel (see Fig. 7) involves altogether $K \times J \times L$=60 000 ODEs in time (arising from the spatial discretization of Eq. (1)). The set of $(N+1) \times K$=400 ODEs in spatial variable x is also five times integrated at each time step (the used method needs 5 evaluations of RHs's per one time step). The algebraic Eqs. (12) and (13) are then solved in each step of the integration of Eqs. (10) and (11) in axial direction.

6. Examples of numerical simulations

The first order kinetic expression was used for the description of CO oxidation in the form:

$$r = k(T_0)\exp\left(-\frac{E}{RT}+\frac{E}{RT_0}\right)c_{CO}\ , \qquad (16)$$

with E/R=12 000 K and k(573 K)=0.06 ms^{-1}.

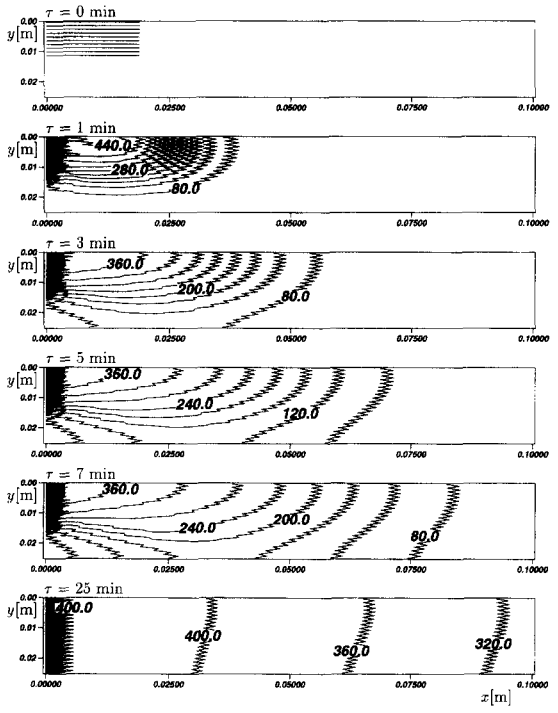

Fig. 8. MC3D1D model, 20 channels in radial direction, evolution of isotherms (°C) on longitudinal half-crossection of the reactor after the central part of solid phase close to the inlet (τ=0) is preheated to 500°C (y=0, reactor axis).

The evolution of temperature field on one half of the longitudinal section of the reactor for the MC3D1D model is shown in Fig. 8. The inlet temperature is 50°C, the inlet CO concentration is 4% vol. The solid phase temperature is initially equal to 50°C with the exception of the central part of the monolith close to the inlet, where the temperature was increased to 500°C. In this case is the energy used for the preheating sufficient for local ignition and the high temperature region spreads subsequently into entire reactor establishing high conversion state over the monolith.

The case, where the initial energy input was sufficient for the ignition is depicted in Fig. 9. Here smaller part of the monolith is preheated than in the first case. Then the region of the increased temperature is blown out of the reactor and the lower conversion stationary state is established over the monolith.

One minute of real time in the model requires about 1 h of the CPU time for the simulation on the HP 735 workstation.

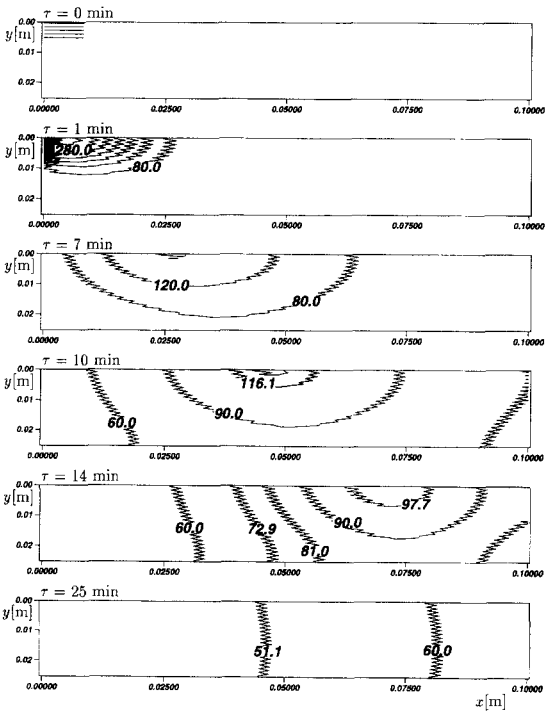

Fig. 9. MC3D1D model, 20 channels in radial direction, evolution of isotherms (°C) on longitudinal half-crossection of the reactor after the central part of solid phase close to the inlet (the heated part of the monolith at τ=0 is smaller than in Fig. 8) is preheated to 500°C (y=0, reactor axis).

7. Conclusions

It was confirmed that the developed channel by channel description of monolith honeycomb reactors is numerically tractable on fast workstation. It enables to determine the evolution of spatiotemporal patterns in the monolith and thus also the comparison with actual temperature profiles in individual monolith channels measured under various conditions. The comparison of such results with the results of experiments and modeling obtained on the basis of the equivalent continuum approach is the subject of future work. The experimental study of gas phase radial temperature profiles in a single channel is also under consideration.

Acknowledgements

This work was partially supported by the grant No. 104/94/0649, Czech Grant Agency, EU COST grant CIPA-CT92-4021 and the grant VS 96073 from the Czech Ministry of Education.

References

[1] A. Cybulski and J.A. Moulin, Catal. Rev. Sci. Eng., 36 (1994) 179.
[2] R. Aris, Models of the catalytic monolith, Proceedings of the 1st Levich Conference, Oxford, 1977.
[3] K. Zygourakis and R. Aris, Heat transfer in the array of passages of monolith reactor, AICHE 75-th Annual Meeting, Los Angeles, CA, 1982.
[4] K. Zygourakis, Chem. Eng. Sci., 44 (1989) 2075.
[5] M. Flytzani-Stephanopulos, G.E. Voecks and T. Charng, Chem. Eng. Sci., 41 (1986) 1203.
[6] D.K.S. Chen, H.S. Oh, E.J. Bissett and D.L. Van Ostrom, A three-dimensional model for the analysis of transient thermal and conversion characteristics of monolithic catalytic converters, SAE Technical paper series 880282, International congress and exposition, Detroit, MI, 29 February–4 March 1988.
[7] R. Jahn, MSc Thesis, Prague Institute of Chemical Technology, Prague, 1996.
[8] L. Dvořák, P. Pinkas and M. Marek, Catal. Today, 20 (1994) 449.
[9] R. Jahn, D. Šnita, M. Kubíček and M. Marek, 1D- 2D- and 3D-modelling of honey-comb reactors, Proc. of 3-rd Workshop on modelling of chemical reaction systems(on CD ROM), Heidelberg, Germany, July 24–26 1996.